Contrib. Astron. Obs. Skalnaté Pleso **48**, 554 – 583, (2018)

Meteoroid stream and meteor showers of comet C/1964 N1. Part II

L. Neslušan[1] **and M. Hajduková, jr.**[2]

[1] *Astronomical Institute of the Slovak Academy of Sciences 059 60 Tatranská Lomnica, The Slovak Republic, (E-mail: ne@ta3.sk)*

[2] *Astronomical Institute of the Slovak Academy of Sciences, Interplanetary Matter Division, Dúbravská cesta 9, 845 04 Bratislava, The Slovak Republic*

Received: September 6, 2018; Accepted: October 9, 2018

Abstract. In this paper we give further, both graphical and tabular, information about our study of the meteor complex of the long-period comet C/1964 N1 (Ikeya). We found that the modeled stream of the comet approaches the Earth's orbit typically in four filaments that correspond to four showers. Their radiant areas are close to the apex of the Earth's motion around the Sun. We confirmed the generic relationship between the studied parent comet and July ξ-Arietids, #533. The comet is probably also the parent of ϵ-Geminids, #23. We suspect that there could be a relationship between the comet and ξ-Geminids, #718, though this relationship is rather uncertain. There are real counterparts of three of the predicted showers in the CAMS and SonotaCo databases.

Key words: Comets: individual: C/1964 N1 (Ikeya) – Meteorites, meteors, meteoroids

1. Introduction

In our previous paper (Neslušan & Hajduková, 2018, henceforth referred to as Paper I) we studied the meteoroid stream originating from the long-period comet C/1964 N1 (Ikeya). In the current paper we give tabular and further graphical information, which was not given in Paper I. For a better identification of predicted and found showers, we compared not only the corresponding geocentric, but also heliocentric radiants, which were both plotted in various coordinate systems. Several of these plots are shown here. With all this information, we intend to give a more complete description of our study of the C/1964 N1's stream.

Let us briefly recapitulate the main results. It was predicted that the C/1964 N1's stream crosses the orbit of our planet ordinarily in four distinct filaments. If some particles were released from the comet's nucleus in the far past, then they can cross the Earth's orbit also in the fifth filament at present. In Paper I, as well as hereinafter, we refer to these filaments as F1 to F4, and F5. Two of the filaments can be identified with the real showers in the meteor databases and the identification of another two is uncertain.

Following the discovery of Šegon et al. (2017), filament F3 was confirmed to be related with the July ξ-Arietids, #533 in the IAU MDC list of all showers[1] (Jopek & Kaňuchová, 2014). Filament F2 was identified with the ϵ-Geminids, #23, and F1 with a poorly defined, yet unknown shower, separated from the IAU MDC CAMS (Gural, 2011; Jenniskens et al., 2011, 2016a,b,c; Jenniskens & Nénon, 2016), and SonotaCo video (SonotaCo, 2009, 2016) databases. And, we suspected a relationship between filament F5 and the shower ξ-Geminids, #718, though this relationship was rather uncertain. The predicted numerousity of the last filament, F4, was low and this was likely the reason why no real counterpart of this filament was found.

Our paper is organized as follows. In Sect. 2, the nominal comet orbit is revisited together with the tool used for the numerical integration of this orbit as well as the orbits of perturbing planets and modeled theoretical particles. In Sect. 3, we give another details about the predicted showers resulting from our simulations. In the fourth section, we give such details about the identification of the predicted showers with their real counterparts and discuss some problems that occurred during the identification. A brief summary of our study is given in Sect. 5.

2. Remarks on the orbit of the parent comet and numerical integration

In our study, we considered the orbit of comet C/1964 N1 with the orbital elements published in the JPL small-body browser (Giorgini et al., 1996)[2]. This orbit, referred to epoch 1964 July 24.0 (JDT = 2438600.5), has the following elements: $q = 0.821752\,\mathrm{au}$, $e = 0.984643$, $a = 53.5099303\,\mathrm{au}$, $\omega = 290.7618^o$, $\Omega = 269.9493^o$, $i = 171.9200^o$, and $T = 2438608.7111$ (1964 August 1.2111).

The positions of the nodes of the nominal orbit during the last 100 millennia can be seen in Fig. 1. We can see the excursions of both post-perihelion (red dots) and pre-perihelion (blue dots) nodes through a large interval of heliocentric distances, from an interior of the Earth's orbit beyond the orbit of Saturn. Both nodes have crossed the orbit of the Earth several times. This implies a possibility that some associated meteor showers can exist.

We recall that the orbit of the parent comet as well as the theoretical particles, and perturbing planets, were integrated by using integrator RA15 (Everhart, 1985) within the software package MERCURY (Chambers, 1999). The gravitational perturbations of eight planets, Mercury to Neptune, were taken into account.

We also recall that the acceleration due to the Poynting-Robertson (P-R, hereinafter) effect is considered in our simulations. In particular, we used the improved formulas derived by Klačka (2014). The usage of them in the case

[1] https://www.ta3.sk/IAUC22DB/MDC2007/
[2] http://ssd.jpl.nasa.gov/sbdb.cgi

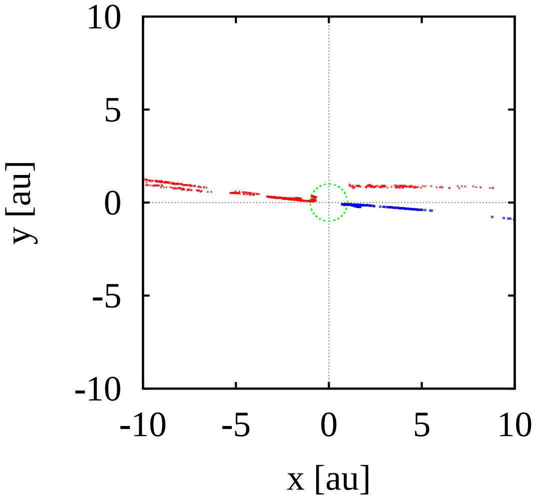

Figure 1. The positions of the orbital nodes of comet C/1964 N1 during the last 100 thousand years. The green circle indicates the orbit of the Earth. The red dots (blue dots) show the positions of ascending (descending) node.
The color version of the figures is provided in the on-line version of the article.

of meteoroid particles was described in, e.g., our previous paper (Hajduková & Neslušan, 2017). The parameter β, being the ratio of the accelerations due to both the P-R effect and gravity of the Sun, is again regarded as a free parameter.

3. The predicted showers

Our way of the modeling of theoretical meteoroid stream associated with the studied comet was described in Paper I. We created several partial models. Each of these was characterized by the evolutionary time t_{ev} and the P-R-effect parameter β. To gain a basic notion about the stream, the basic set of our models consisted of the models with every combination of values t_{ev} = 5, 10, 20, 40, and 80 kyr, and β = 0.00001, 0.0001, 0.001, 0.003, 0.005, 0.007, and 0.009. For some values of evolutionary time, the P-R effect caused a deflection of the stream from the collisional course with the Earth earlier or later than for the initially last considered value of $\beta = 0.009$. During the search of when the effect is strong enough to cause the complete deflection, we also created a few models with other values of β than listed above (β = 0.006, 0.008, 0.010, and 0.011).

We followed the dynamical evolution of the created stream until present. An overall view of the positions of the geocentric radiants of theoretical particles that approach the Earth's orbit within the distance of 0.05 au at present is shown in Fig. 2a, in an example (model for $(t_{ev},\ \beta) = (20,\ 0.0001)$). When these positions are shown in the ecliptical coordinate system with the origin identical to the apex of the Earth's motion around the Sun (the ecliptic longitude of every radiant, λ, is replaced with the longitude λ_2 calculated according to the relation $\lambda_2 = \lambda - (\lambda_\odot + 270^o)$; $\lambda_\odot$ is the solar longitude of meteor) - see an example in Fig. 2b - we see that the radiant areas of all filaments are in the close vicinity of the apex. This means that all the areas are also close to the ecliptic.

We can observe a rough symmetry of the filaments F1 and F4, as well as F2 and F3, in respect to the Earth's apex (Fig. 2b). The majority of radiants of a given filament are in a single quadrant (four filaments, F1−F4, in four quadrants) of the modified ecliptical coordinate system. However, the distribution to specific quadrants is not exact. There is some "contamination" of radiants of filament F4 in the radiant area of F3.

The detailed distribution of the positions of heliocentric radiants of the particles approaching the Earth's orbit within 0.05 au at present can be seen in Fig. 3 for four models. The radiants are distributed on both sides of the ecliptic (Fig. 3a,b,e,f). Sometimes, the radiant areas touch each other. Because of this circumstance, we also analyzed the distribution of radiants in dependence on the ecliptic longitude (Fig. 3c,d,g,h). A double-peak distribution is seen as for the radiants situated southward as those northward of the ecliptic, in the most models.

Just these double-peaked distributions were the reason why we divided the stream mostly into four filaments, two (F1 and F2) with the radiants northward and two (F3 and F4) southward of the ecliptic. The border between two neighboring filaments is the minimum between the peaks in the ecliptic-longitude distribution and, of course, the filaments are also separated by the ecliptic. In a few models for $t_{ev} = 80$ kyr and high values of β ($\beta = 0.005$, 0.007, 0.009, and 0.010), only a single "southern" filament occurred (Fig. 3f,h). As mentioned in Sect. 1, we refer to this filament as F5 and discuss its occurrence in Sect. 4.3. The mean characteristics of the predicted showers are given in Tables 1 and 2.

In Figs. 4 and 5, the positions of the geocentric and heliocentric radiants of theoretical particles and the corresponding real showers are shown in some models. In particular, the plots of Fig. 4 are related to filament F3 in the models with the P-R-effect parameter $\beta = 0.00001$ and a series of evolutionary times, t_{ev}. In the left-hand plots, there are the geocentric radiants. We can see a shift of some of these radiants to positions with a larger right ascension and declination and, at the same time, larger dispersion of the radiants. As it could be expected, the radiant area is more dispersed in the models where the meteoroid orbits evolve a longer time. The larger dispersion also occurs at the heliocentric radiants which are shown in the right-hand plots. The heliocentric radiants are more compact than their geocentric counterparts. With the increasing t_{ev}, the radiant area of the heliocentric radiants becomes larger, but its center, i.e. the mean radiant, remains the same.

The radiants in Fig. 5 are related to filament F2 in the models for t_{ev} = 40 kyr and a series of the values of β-parameter. We can see influence of the P-R effect on the dynamics of particles in this filament. The effect tends to move the particles away from the vicinity of the Earth's orbit, therefore there is a smaller number of radiants in the radiant area with the increasing value of β. Again, the positions of the geocentric radiants are shown in the left-hand plots. We can see there a gradual shift of the radiant area to smaller values of right ascension. A highly concentrated area of numerous heliocentric radiants, in the right-hand plots, occur up to $\beta = 0.005$. For larger β-values the concentration sharply decreases.

In Paper I we showed the positions of the geocentric radiants in some of the models with the radiants shown in Figs. 4 and 5 in the sun-centered ecliptic coordinates (Figs. 3 and 4 in Paper I). The increasing of dispersion and decreasing of the concentration can also be seen in these plots.

We recall that we constructed the plots like those in Figs. 4 and 5 for every filament in each model, where the identification of a predicted shower with a real shower separated at least from a single database considered was successful. Except for tabular data, these figures also served to remove some identifications, which seemed to be successful on the basis of the D-criterion, but the predicted and observed radiant areas occurred unacceptably different (a more detailed description about the identification is given in Sect. 4).

The radiants of some theoretical particles situated clearly outside the heliocentric radiant area, that were removed from a given filament in this step, occurred to be merged and, thus, indistinguishable from the filament, when the geocentric radiant area was constructed. Hence, the comparison between the heliocentric, instead of geocentric, predicted and real radiants may sometimes result in some improvement (not, however, exceeding the statistical uncertainity at the determination of mean characteristics).

According to Fig. 5 (and others, not shown), there is, mostly, no perfect match between a given prediction and a real shower. Neither does the P-R effect tend to improve the match significantly. The latter implies that the meteoroid particles in the C/1964 N1 stream are, likely, quite large and the effect on them is not very efficient. In more detail, a good match can be found, typically, for β up to the value of about 0.001.

4. Identification of the predicted and real showers

The mean orbits of predicted meteor showers were used as the initial orbits in the iteration, done within the break-point method, to separate the eventual real counterparts of the showers from the meteor catalogs considered. The mean characteristics of these real showers are listed in Tables 3 and 4. Unfortunately, the dependence $N = N(D_{lim})$ constructed within the method never exhibited a clear break point; therefore, it was hard to decide if the separated set of meteors

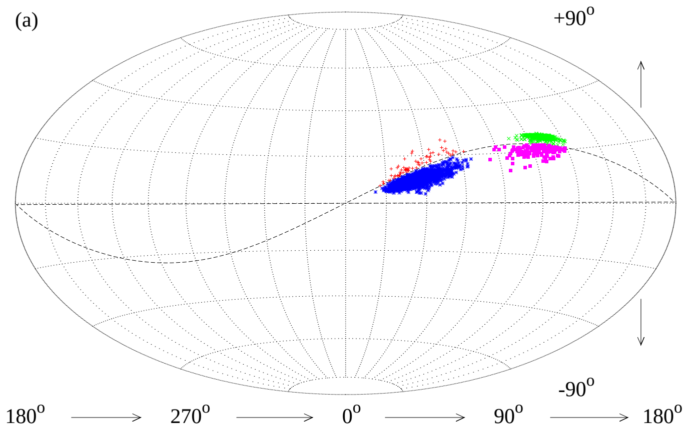

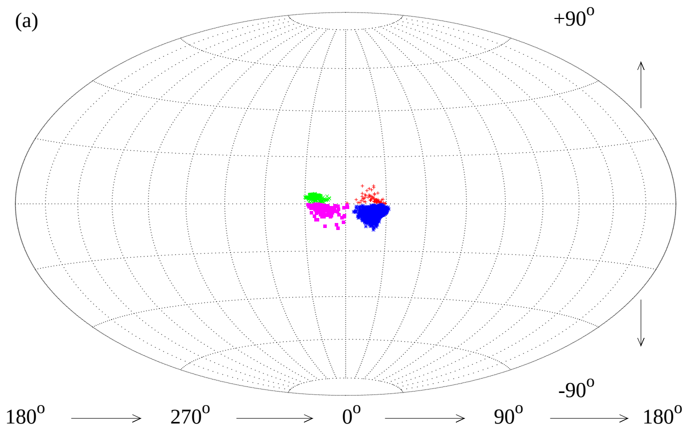

Figure 2. Positions of radiants of theoretical particles grouped in four filaments of the meteoroid stream associated with comet C/1964 N1 in the equatorial coordinate frame (plot a) and the ecliptical coordinate frame with the ecliptic longitude shifted in such a way that the apex of the Earth's motion is in the origin of the coordinate system (plot b). The radiants of particles in the F1 (F2, F3, F4) filament are plotted with red plus-shape points (green crosses, blue asterisks, violet full squares). The radiant positions are shown for the model of the C/1964 N1 stream characterized by $(t_{ev},\ \beta) = (20,\ 0.0001)$. The sinusoid-like curve in plot (a) shows the ecliptic.

is actually a shower or only a random, moderate accumulation of meteors in the given part of the orbital phase space. Hence, one should be careful in regarding the mean orbits of separated showers, listed in Tables 3 and 4, as actually real.

As well, the relationship between the predicted and separated showers is mostly uncertain. We recall (what was already stated in Paper I) that the iteration often resulted in the real mean orbit that was considerably different from the predicted mean orbit. We calculated the Southworth-Hawkins D-discriminant between the predicted and corresponding real mean orbits and we excluded all separated mean orbits with $D_{SH} > 0.2$. We also discarded some separated real showers if their geophysical data were much too different from the predicted counterpart. In particular, we mean that the difference in the mean solar longitude can scarcely exceed $\sim 20^o$, or the position of the predicted mean radiant should be away from its real counterpart more than a dozen of degrees.

We also calculated the D-discriminant between every predicted and known orbit in the IAU MDC list of all showers and we regarded as, possibly, related only the orbits with $D_{SH} \leq 0.20$. These identifications are given in Table 5. (When we used $D_{SH} < 0.25$, there occurred only a singe orbit, in addition, and this is also listed in the parentheses in Table 5.)

Criterion $D_{SH} \leq 0.20$ is not very strict, therefore it is not surprising that a single real shower, regardless it was separated from a considered database or found in the IAU MDC list of showers, is identified with more than a single predicted filament. Fortunately, the search for the minimum value of D_{SH} between the given real shower and a predicted filament leads to a unique association of the shower and filament.

4.1. Filaments F3 and F1, July ξ-Arietids

Seeing the values of the Southworth-Hawkins D-discriminant in the last but one column of the first part of Table 5, we can well identify the theoretical filament F3 to the shower July ξ-Arietids, #533 in the IAU MDC list of showers. This identification is consistent with the result obtained by Šegon et al. (2017). As seen in Table 5, the similarity between the mean orbit of the July ξ-Arietids and the predicted mean orbit of F3 can be characterized with a very small value of the D-discriminant. Specifically, $D_{SH} = 0.053$ when we consider the mean orbit determined by Šegon et al. (2014) and $D_{SH} = 0.070$ when the mean orbit determined by Jenniskens et al. (2016c) is considered. A little larger value, $D_{SH} = 0.078$, characterizes the similarity when we compare our filament F3 and the mean orbit found by Kornoš et al. (2014b).

A real shower corresponding to filament F3, its models especially for $t_{ev} =$ 20 kyr, was also found in the SonotaCo video data, whereby three modifications, denoted by 3S, 30S, and 32S in Table 3, most probably of the same shower, were separated by the break-point method in relation with F3. In addition, the shower 25C separated from the IAU MDC CAMS data is in agreement with F3 for $t_{ev} \geq 40$ kyr. No shower corresponding to F3 was found in the IAU MDC photographic (Porubčan et al., 2011; Neslušan et al., 2014) and EDMOND video (Kornoš et al., 2014a,b) data sets.

Comparing the predicted filament F3 to the real showers, it seems that the real meteoroids were not much influenced by the P-R effect. Their size corresponds to $\beta \lessapprox 0.001$. From Fig. 4 we can conclude that the evolutionary period of the particles in this filament was likely longer than 5 kyr, but shorter than ~80 kyr, since the predicted radiant area is much more dispersed than its observed counterpart for $t_{ev} = 80$ kyr.

The radiant area of filament F3 is situated below the projection of the ecliptic on the celestial sphere. Filament F1 has a very similar mean orbit, but its radiant area is situated northward of the ecliptic. Hence, F1 can be regarded as a northern branch of the southern F3. Some showers with the mean characteristics resembling those of F1 were found in the IAU MDC CAMS video (showers 13C, 15C, and 17C), as well as in the SonotaCo video databases (10S; see Tables 1 and 2). However, these real showers were predicted only with the help of models with $t_{ev} = 80$ and are very dispersed. They are also uncertain due to a high threshold D_{lim}, from 0.32 to 0.40, used for their separation. Shower 13C was predicted for $\beta \leq 0.001$, 15C only for $\beta = 0.003$, 17C only for $\beta = 0.007$, and 10S for $\beta = 0.007$ and 0.009. No shower in the IAU MDC list was identified with F1.

4.2. Filaments F2 and F4, ϵ-Geminids

Filament F2 has probably its counterpart in the IAU MDC CAMS data - modifications 14C, 18C, 24C, and 26C. The match is quite good for all of them. Furthermore, we found a certain similarity of the mean orbit of F2 with three modifications, 20S, 22S, and 24S, in the SonotaCo data. We must be, however, careful with this identification, since the predicted solar longitude is up to 20^o larger than observed one in the case of 20S, and the observed one is about 20^o larger than predicted one in the case of 22S. The level of match of the predicted and real heliocentric radiant positions in F2 can be seen in Fig. 5, where these positions are shown in the models for $t_{ev} = 40$ kyr and a series of the values of the P-R-effect parameter β.

Filament F4 is the southern branch of the northern F2. Any real counterpart of F4 was found neither in the considered databases, nor in the IAU MDC list of all showers.

4.3. Filament F5

As seen in Fig. 3f,h, filaments F3 and F4, with the radiant areas below the ecliptic, disappeared and, instead of these filaments, there occurred a single filament, F5, with the radiant area in the region near the border of F3 and F4. This behavior can be observed in the theoretical models for $t_{ev} = 80$ kyr and $\beta \geq 0.005$ ($\beta = 0.007$ in Fig. 3f,h).

In Paper I we stated that the occurrence of the "irregular" filament F5 is, most likely, the consequence of a considerable change of the inclination of the parent-comet orbit. (This can be observed in Fig. 1f in Paper I.) In the period from about −92 to −80 kyr, the inclination was decreased, from $\sim 170^o$ to $\sim 158^o$ (i.e. the absolute value of inclination was increased from $\sim 10^o$ to $\sim 22^o$; the orbit was at a larger distance from the ecliptic).

Because of this circumstance, we created additional stream models for the sequence of values t_{ev} equal to 50, 60, 70, 75, 78, 82, 85, and 90 kyr and $\beta = 0.007$ (since filament F5 in the models for $t_{ev} = 80$ kyr is the most abundant in the model for $\beta = 0.007$). As stated in Paper I, only if we consider particles released from the parent 80, 78, 70, and 60 kyr ago, some of them dynamically evolved to the present-day filament F5 and/or other filaments. Hence, only the corresponding data for these models are given in Tables 1 and 2.

We recall that no real counterpart of F5 was separated in the considered databases. We found only a rough similarity of its mean characteristics with the mean characteristics of ξ-Geminids, #718 in the IAU MDC list, which were found by Jenniskens et al. (2016a).

5. Summary

We gave additional details of our study, with the main results already published in Paper I, in which we modeled a theoretical stream of the comet C/1964 N1 (Ikeya). Our simulations of the comet's stream imply the existence of, basically, four distinct filaments of the stream, which can be observed in the Earth's atmosphere as four individual showers. We label the filaments as F1 to F4.

We further found that the orbit of the parent comet and its stream rapidly evolved in a period that ended about 50 kyr ago. During this period, the orbital corridors of individual filaments occupied a different space. One of the filaments, F5, was predicted to cross, temporarily, the Earth's orbit in a different arc of its orbit than the younger filaments F1 to F4.

In the current paper we gave the further graphical and tabular information, which shows in more detail that the separation of real showers corresponding to the predicted ones was often not unique. Starting the iteration procedure from different initial orbits, we obtained several modifications of, most probably, the same real shower - cf. the first and last columns in Tables 3 and 4. In these tables, one can also see that the separated real showers contain a small number of members, 28 at most, many of them consist of 10 or fewer members.

Filament F3 was well identified with the shower July ξ-Arietids, #533 (Šegon et al., 2014, 2017, this work). In this work, filament F2 was identified to ϵ-Geminids, #23. A real counterpart of F1 was found in the CAMS and also SonotaCo data. And, we suspected that filament F5 could, perhaps, be related to the ξ-Geminids, #718. No real counterpart of filament F4 was found in the databases used, or in the IAU MDC list of showers.

The positive identifications of filament F1 in the data for $t_{ev} = 80\,\mathrm{kyr}$ (Table 1 or 2) imply a relatively large evolutionary age of meteoroids in F1 of $\sim$80 kyr. The age of the particles in F2 should be $\sim$20 and more millennia, the age of the largest part is predicted to be around $\sim$40 kyr. Filament F3 can contain some older as well as very young meteoroids, which were only recently released from the surface of the parent. The age of meteoroids in this filament does not likely much exceeds $\sim$40 kyr. Later, the stream seems to be more and more deflected from the collisional course with the Earth.

Filaments F1 to F4 should mostly contain the relatively large particles corresponding to the P-R parameter $\beta \lesssim 0.001$; more detailed information can be discerned from Table 1, giving the predicted numbers for the specific values of β. Only filament F5, if its real counterpart exists, contains the Earth-hitting particles that are small, corresponding to $0.005 \lesssim \beta \lesssim 0.010$.

Our study provides an evidence that the comet C/1964 N1 is an active parent body of at least one, possibly more real showers. At the moment, there are not enough sufficient bulk of the precise data. We believe that the stream of the comet will be studied again in the future, when more extensive meteor data will be collected.

Acknowledgements. The work was supported, in part, by the VEGA - the Slovak Grant Agency for Science, grant No. 2/0037/18, and by the Slovak Research and Development Agency under the contract No. APVV-16-0148.

References

Chambers, J. E., A hybrid symplectic integrator that permits close encounters between massive bodies. 1999, *Mon. Not. R. Astron. Soc.*, **304**, 793, DOI: 10.1046/j.1365-8711.1999.02379.x

Cook, A. F., A Working List of Meteor Streams. 1973, *NASA Special Publication*, **319**, 183

Everhart, E., An efficient integrator that uses Gauss-Radau spacings. 1985, in *Dynamics of Comets: Their Origin and Evolution, Proceedings of IAU Colloq. 83, held in Rome, Italy, June 11-15, 1984. Edited by Andrea Carusi and Giovanni B. Valsecchi. Dordrecht: Reidel, Astrophysics and Space Science Library. Volume 115, 1985, p.185*, ed. A. Carusi & G. B. Valsecchi, 185

Giorgini, J. D., Yeomans, D. K., Chamberlin, A. B., et al., JPL's On-Line Solar System Data Service. 1996, in Bulletin of the American Astronomical Society, Vol. **28**, *AAS/Division for Planetary Sciences Meeting Abstracts #28*, 1158

Gural, P. S., The California All-sky Meteor Surveillance (CAMS) System. 2011, in *Proceedings of the International Meteor Conference, 29th IMC, Armagh, Northern Ireland, 2010*, 28–31

Hajduková, M. & Neslušan, L., Regular and transitory showers of comet C/1979 Y1 (Bradfield). 2017, *Astron. Astrophys.*, **605**, A36, DOI: 10.1051/0004-6361/201730646

Jenniskens, P., Meteor Showers Validated by Cameras for Allsky Meteor Surveillance (CAMS). 2012, in LPI Contributions, Vol. **1667**, *Asteroids, Comets, Meteors 2012*, 6339

Jenniskens, P., Gural, P. S., Dynneson, L., et al., CAMS: Cameras for Allsky Meteor Surveillance to establish minor meteor showers. 2011, *Icarus*, **216**, 40, DOI: 10.1016/j.icarus.2011.08.012

Jenniskens, P. & Nénon, Q., CAMS verification of single-linked high-threshold D-criterion detected meteor showers. 2016, *Icarus*, **266**, 371, DOI: 10.1016/j.icarus.2015.10.004

Jenniskens, P., Nénon, Q., Albers, J., et al., The established meteor showers as observed by CAMS. 2016a, *Icarus*, **266**, 331, DOI: 10.1016/j.icarus.2015.09.013

Jenniskens, P., Nénon, Q., Gural, P. S., et al., CAMS confirmation of previously reported meteor showers. 2016b, *Icarus*, **266**, 355, DOI: 10.1016/j.icarus.2015.08.014

Jenniskens, P., Nénon, Q., Gural, P. S., et al., CAMS newly detected meteor showers and the sporadic background. 2016c, *Icarus*, **266**, 384, DOI: 10.1016/j.icarus.2015.11.009

Jopek, T. J. & Kaňuchová, Z., Current status of the˜IAU MDC Meteor Showers Database. 2014, *Meteoroids 2013*, 353

Klačka, J., Solar wind dominance over the Poynting-Robertson effect in secular orbital evolution of dust particles. 2014, *Mon. Not. R. Astron. Soc.*, **443**, 213, DOI: 10.1093/mnras/stu1133

Kornoš, L., Koukal, J., Piffl, R., & Tóth, J., EDMOND Meteor Database. 2014a, in *Proceedings of the International Meteor Conference, Poznan, Poland, 22-25 August 2013*, ed. M. Gyssens, P. Roggemans, & P. Zoladek, 23–25

Kornoš, L., Matlovič, P., Rudawska, R., et al., Confirmation and characterization of IAU temporary meteor showers in EDMOND database. 2014b, *Meteoroids 2013*, 225

Neslušan, L. & Hajduková, Jr., M., Meteor showers of comet C/1964 N1 (Ikeya). 2018, *Astron. Astrophys.*, **616**, A162, DOI: 10.1051/0004-6361/201832829

Neslušan, L., Porubčan, V., & Svoreň, J., IAU MDC Photographic Meteor Orbits Database: Version 2013. 2014, *Earth Moon and Planets*, **111**, 105, DOI: 10.1007/s11038-013-9427-1

Porubčan, V., Svoreň, J., Neslušan, L., & Schunová, E., The Updated IAU MDC Catalogue of Photographic Meteor Orbits. 2011, in *Meteoroids: The Smallest Solar System Bodies*, ed. W. J. Cooke, D. E. Moser, B. F. Hardin, & D. Janches, 338

SonotaCo, A meteor shower catalog based on video observations in 2007-2008. 2009, *WGN, Journal of the International Meteor Organization*, **37**, 55

SonotaCo, Observation error propagation on video meteor orbit determination. 2016, *WGN, Journal of the International Meteor Organization*, **44**, 42

Šegon, D., Gural, P., Andreić, Ž., et al., New showers from parent body search across several video meteor databases. 2014, *WGN, Journal of the International Meteor Organization*, **42**, 57

Šegon, D., Vaubaillon, J., Gural, P. S., et al., Dynamical modeling validation of parent bodies associated with newly discovered CMN meteor showers. 2017, *Astron. Astrophys.*, **598**, A15, DOI: 10.1051/0004-6361/201629100

A. Appendix: Further graphical and tabular results

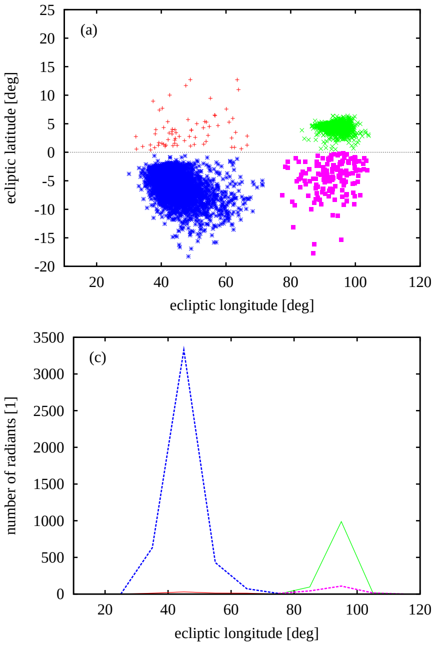

Figure 3. Positions of heliocentric radiants of theoretical particles grouped into five filaments of the meteoroid stream associated with comet C/1964 N1 (plots a, b, e, and f) and distribution of these radiants in the ecliptic longitude (plots c, d, g, and h). The radiants of particles in the F1 (F2, F3, F4, F5) filament are plotted with red plus-shape points (green crosses, blue asterisks, violet full squares, cyan full circles). The distribution of radiants situated northward (southward) from the ecliptic is shown with a red and green solid (blue and violet dashed; in plot (h) cyan dashed) curve. (The color of the part of the curve is the same as the radiant positions in the corresponding plot showing the positions of the radiants.) Both positions and distributions are shown for four models of the C/1964 N1 stream characterized by (t_{ev}, β) equal to (20, 0.0001) (plots a and c), (40, 0.003) (b, d), (80, 0.00001) (e, g), and (80, 0.007) (f, h). To show the positions of radiants, the ecliptical coordinate frame is used. Plots e−h are shown on the next page.

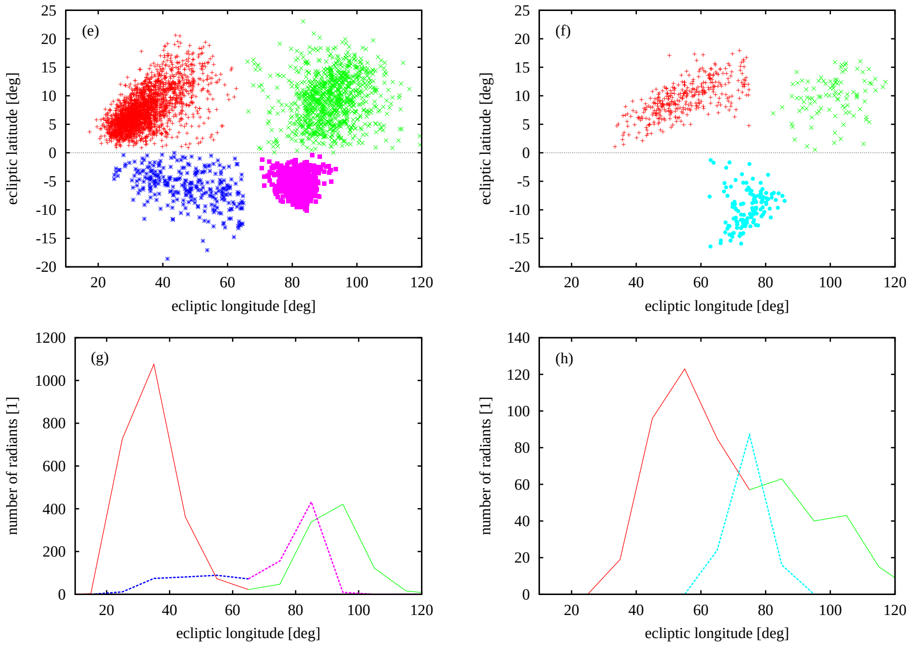

Figure 3. – continued.

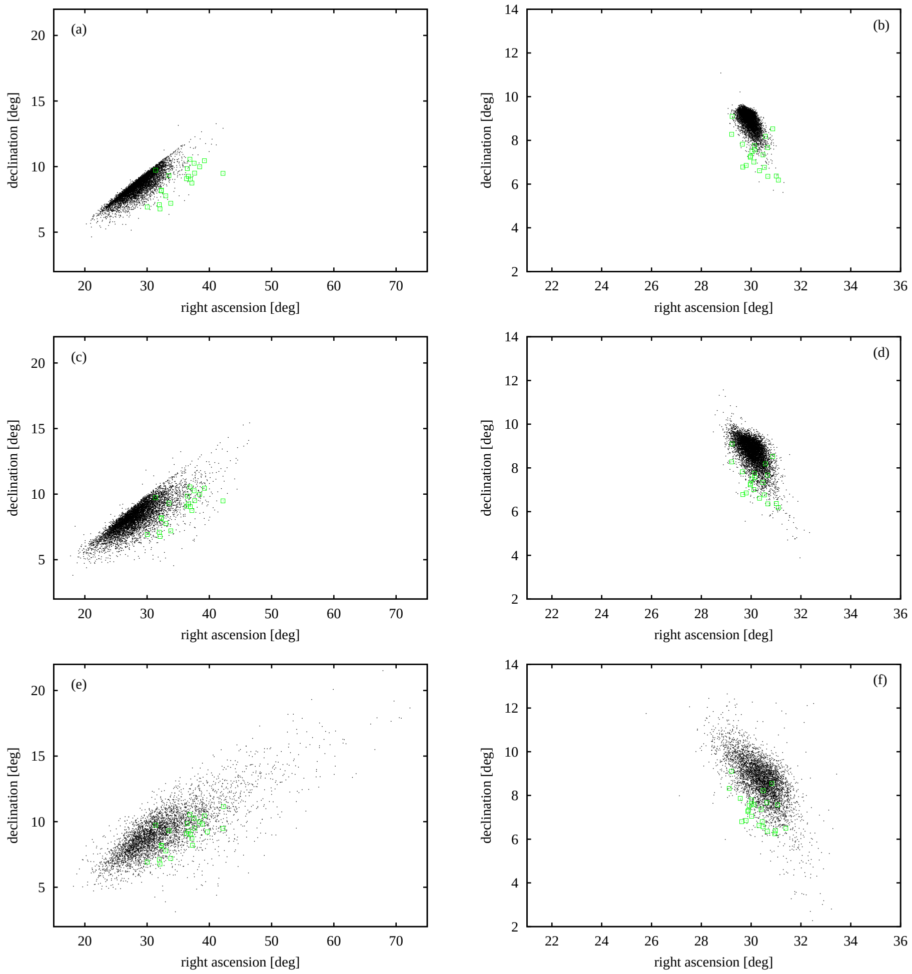

Figure 4. Positions of geocentric (left-hand plots, a, c, e, g, and i) and heliocentric (right-hand plots, b, d, f, h, and j) radiants of theoretical particles (black dots) in the predicted filament F3 and corresponding real-shower meteors separated from the CAMS-video (blue asterisks) and SonotaCo-video (green empty squares) databases. The positions are shown in the models for the P-R-effect parameter $\beta = 0.00001$ and a series of evolutionary times $t_{ev} = 5$ (plots a and b), 10 (c, d), 20 (e, f), 40 (g, h), and 80 kyr (i, j). Plots g−j are shown on the next page.

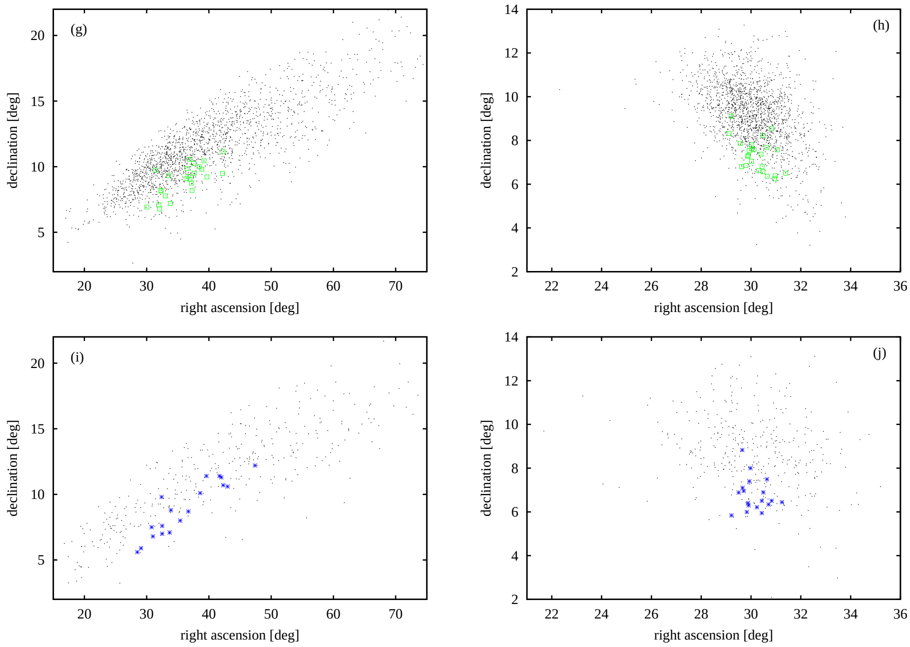

Figure 4. – continued.

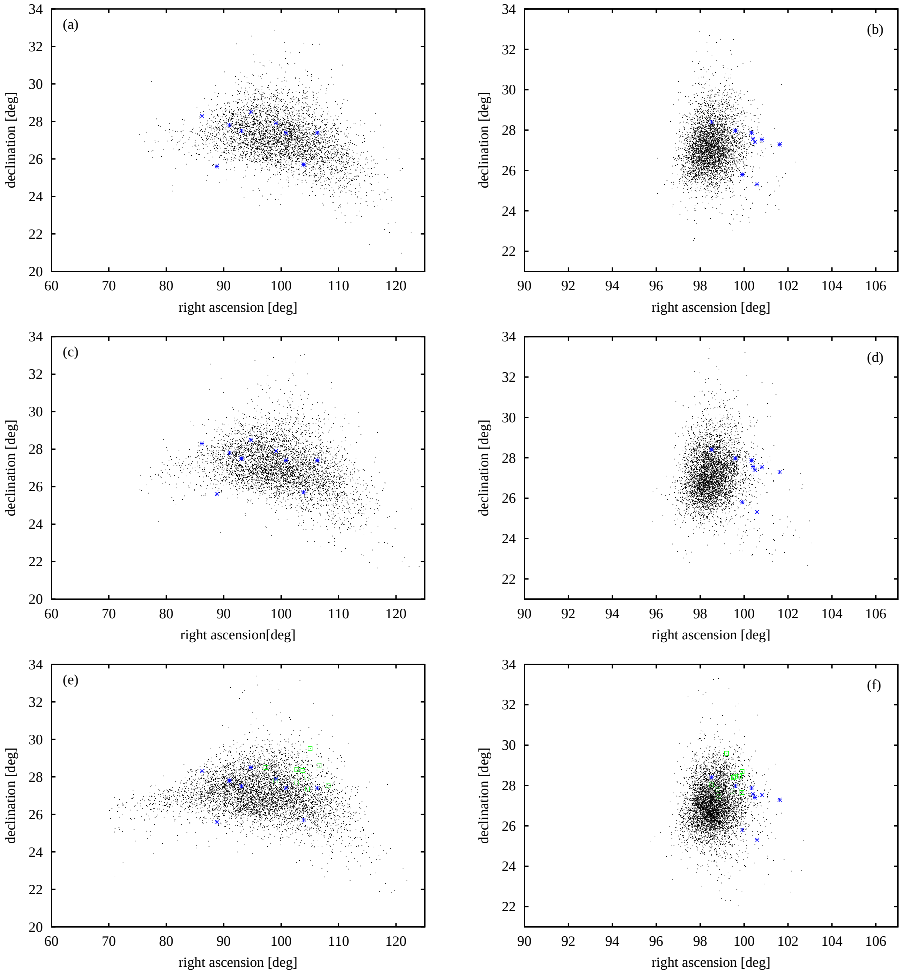

Figure 5. Positions of geocentric (right-hand plots, a, c, e, g, i, k, and m) and heliocentric (right-hand plots, b, d, f, h, j, l, and n) radiants of theoretical particles (black dots) in the predicted filament F2 and corresponding real-shower meteors separated from the CAMS-video (blue asterisks) and SonotaCo-video (green empty squares) databases. The positions are shown in the models for the evolutionary time $t_{ev} = 40\,\mathrm{kyr}$ and a series of the values of P-R-effect parameter $\beta = 0.00001$ (plots a and b), 0.0001 (c, d), 0.001 (e, f), 0.003 (g, h), 0.005 (i, j), 0.007 (k, l), and 0.008 (m, n). Plots g–n are shown on the next page.

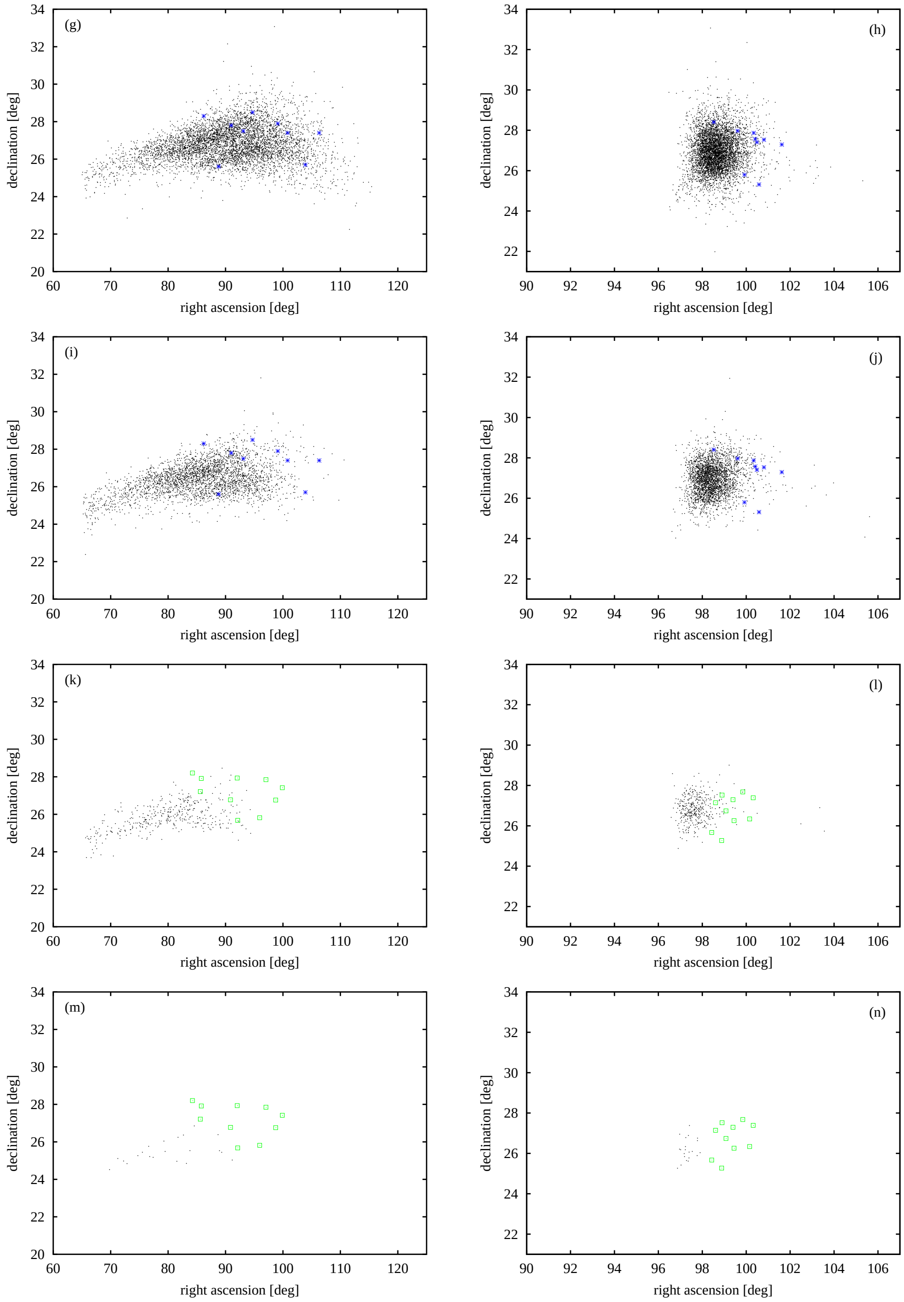

Figure 5. − continued.

Table 1. The mean geophysical characteristics of the predicted meteor showers. Notes: t_{ev} - the period following the orbital evolution (the theoretical stream was modeled before this time); β - the parameter characterizing the strength of the P-R effect; $\lambda_{\odot}$ - the mean solar longitude corresponding to the expected maximum of a shower; α and δ - equatorial coordinates of the mean geocentric radiant; V_g and V_h - the mean geocentric and heliocentric velocity; γ - the angular distance of the mean radiant from the Sun at the time corresponding to the $\lambda_{\odot}$ of the maximum; N_s - the number of particles in the orbits approaching the Earth's orbit within 0.05 au; D_{lim} - the threshold value of the Southworth-Hawkins D-discriminant used to separate the meteors of the filament; i.r.s. - the real shower identified with a given filament in a given model (according to this identification number, the real shower can be found in Tables 3 and 4). Time t_{ev} is given in kilo-years, the angular quantities are given in degrees, and velocities in km s^{-1}.

t_{ev}	β	$\lambda_{\odot}$	α	δ	V_g	V_h	γ	N_s	D_{lim}	i.r.s.
				filament F1						
10	0.0001	104.2± 7.5	27.9± 5.8	12.7± 2.0	68.9± 0.3	41.6± 0.1	74.	6	0.14	–
20	0.00001	117.3± 11.9	37.7±C 9.1	16.3± 3.4	69.5± 0.5	41.5± 0.1	77.	59	0.24	–
20	0.0001	115.9± 14.8	36.2± 11.1	16.4± 4.4	69.4± 0.7	41.6± 0.1	77.	67	0.27	–
20	0.001	115.3± 11.9	35.8± 9.0	16.2± 3.5	69.5± 0.5	41.6± 0.1	77	31	0.18	–
20	0.003	126.9± 18.2	44.6± 14.2	18.0± 3.7	69.9± 0.6	41.5± 0.1	80.	18	0.23 –	
40	0.00001	137.0± 19.5	52.1± 14.1	21.1± 4.1	70.2± 0.8	41.6± 0.2	82.	166	0.32	–
40	0.0001	127.1± 15.2	45.6± 11.9	18.9± 3.7	69.8± 0.6	41.6± 0.1	79.	108	0.23	–
40	0.001	138.5± 16.7	51.8± 11.7	21.5± 3.3	70.5± 0.7	41.7± 0.2	84.	134	0.28	–
40	0.003	135.3± 12.0	47.1± 8.7	20.9± 2.4	70.8± 0.4	41.8± 0.1	85.	917	0.13	–
40	0.005	133.8± 11.5	45.7± 8.2	20.5± 2.3	70.8± 0.4	41.8± 0.1	85	2059	0.12	–
40	0.007	133.0± 11.1	45.0± 7.7	20.2± 2.3	70.8± 0.4	41.8± 0.1	85.	1286	0.14	–
40	0.008	132.0± 11.4	44.0± 7.8	19.9± 2.3	70.8± 0.4	41.8± 0.1	85.	346	0.13	–
50	0.007	125.2± 10.0	39.5± 7.1	18.4± 2.2	70.5± 0.3	41.7± 0.1	82.	2356	0.19	20S
60	0.007	103.1± 7.9	23.3± 5.4	11.8± 1.9	69.8± 0.4	41.8± 0.0	77.	27	0.11	–
70	0.007	110.4± 8.9	28.7± 6.6	14.9± 2.9	69.9± 0.4	41.7± 0.1	78.	1514	0.23	–
80	0.00001	98.9± 12.1	20.6± 8.6	13.4± 4.7	69.0± 0.6	41.7± 0.1	75.	2248	0.32	13C
80	0.0001	99.7± 12.6	21.2± 9.2	13.7± 4.8	69.0± 0.6	41.7± 0.1	75.	2306	0.38	13C
80	0.001	105.6± 15.6	25.7± 11.8	15.7± 5.8	69.3± 0.6	41.7± 0.1	76.	2103	0.40	13C
80	0.003	120.0± 17.1	37.4± 14.1	20.9± 5.8	69.6± 0.5	41.7± 0.1	78.	1903	0.40	15C

Table 1. − continued.

t_{ev}	β	$\lambda_\odot$	α	δ	V_g	V_h	γ	N_s	D_{lim}	i.r.s.
				filament F1 − continuation						
80	0.005	127.5± 17.6	44.2± 15.2	22.9± 5.2	69.8± 0.5	41.7± 0.1	79	1362	0.37	16C
80	0.007	133.1± 19.7	49.5± 17.1	23.7± 5.1	70.0± 0.5	41.7± 0.1	80.	442	0.38	17C, 10S
80	0.009	130.8± 13.7	47.1± 12.1	22.5± 4.7	70.1± 0.4	41.7± 0.0	80	67	0.32	10S
80	0.010	135.9± 27.8	49.1± 22.5	20.1± 5.9	70.4± 0.6	41.7± 0.2	84	10	0.28	–
				filament F2						
10	0.00001	217.0± 2.6	112.1± 2.1	24.6± 0.4	69.7± 0.2	42.2± 0.0	107	79	0.06	–
10	0.0001	216.4± 2.4	111.7± 1.9	24.7± 0.3	69.7± 0.1	42.2± 0.0	107.	77	0.17	–
10	0.001	215.5± 2.3	110.9± 1.9	24.8± 0.3	69.8± 0.1	42.2± 0.0	107	134	0.06	–
10	0.003	214.4± 1.6	109.9± 1.4	25.0± 0.2	69.8± 0.1	42.2± 0.0	106	170	0.06	–
10	0.005	214.1± 1.4	109.5± 1.1	25.1± 0.1	69.8± 0.1	42.2± 0.0	106	64	0.03	–
20	0.00001	211.6± 5.2	108.1± 4.2	25.5± 0.7	70.0± 0.2	42.2± 0.1	105.	1067	0.23	18C
20	0.0001	211.2± 5.1	107.8± 4.1	25.5± 0.7	70.0± 0.3	42.1± 0.1	105.	1103	0.18	18C
20	0.001	209.7± 5.1	106.5± 4.2	25.8± 0.6	70.1± 0.2	42.2± 0.0	105.	1441	0.18	18C
20	0.003	206.5± 5.0	103.7± 4.1	26.1± 0.5	70.2± 0.2	42.1± 0.0	104	1689	0.15	14C
20	0.005	204.4± 4.1	101.8± 3.3	26.4± 0.3	70.3± 0.2	42.1± 0.0	104.	721	0.13	14C
20	0.006	202.7± 4.2	100.3± 3.5	26.6± 0.2	70.3± 0.2	42.2± 0.0	103.	239	0.10	14C
40	0.00001	201.7± 8.1	100.0± 6.9	27.1± 1.3	70.3± 0.3	42.1± 0.1	103.	4059	0.21	14C
40	0.0001	201.3± 8.1	99.7± 6.9	27.1± 1.3	70.3± 0.3	42.1± 0.1	103.	4361	0.24	14C
40	0.001	197.5± 9.3	96.8± 7.6	28.1± 8.3	69.8± 5.2	42.5± 3.4	101.	5074	0.22	14C, 24S
40	0.003	190.7± 9.7	90.8± 8.2	26.8± 1.0	70.7± 0.3	42.0± 0.1	100.	5379	0.21	14C
40	0.005	185.2± 9.2	86.3± 7.7	26.4± 0.9	70.9± 0.2	42.0± 0.1	99.	2894	0.20	14C
40	0.007	178.1± 8.6	80.3± 6.9	25.9± 0.7	71.0± 0.2	42.0± 0.1	97.	347	0.14	20S
40	0.008	178.4± 7.9	80.1± 6.3	25.5± 0.6	71.0± 0.2	42.0± 0.1	97.	21	0.08	20S
50	0.007	181.4± 9.5	83.7± 7.8	25.7± 1.1	71.0± 0.2	41.9± 0.1	97.	544	0.20	14C, 20S
70	0.007	188.8± 9.8	89.6± 8.3	25.8± 1.2	70.8± 0.2	42.0± 0.1	99.	110	0.19	14C, 20S
80	0.00001	202.2± 12.8	102.4± 10.9	28.2± 2.6	70.3± 0.4	42.0± 0.1	101.	953	0.39	18C, 22S
80	0.0001	203.5± 11.0	103.3± 9.6	28.1± 2.6	70.3± 0.4	42.0± 0.1	102.	999	0.38	22S, 18C
80	0.001	203.1± 12.4	103.7± 10.7	28.1± 2.7	70.4± 0.4	42.0± 0.1	101.	1137	0.39	22S, 18C
80	0.003	200.6± 16.3	104.6± 13.2	28.8± 2.8	70.6± 0.4	42.0± 0.1	98.	1074	0.40	23C

Table 1. - continued.

t_{ev}	β	$\lambda_{\odot}$	α	δ	V_g	V_h	γ	N_s	D_{lim}	i.r.s.
				filament F2 − continuation						
80	0.005	200.3± 14.8	107.1± 12.4	29.0± 2.6	70.9± 0.3	41.9± 0.1	95	462	0.40	24C
80	0.007	202.7± 11.2	108.8± 9.1	27.9± 2.4	71.0± 0.3	41.9± 0.1	96.	98	0.38	24C
80	0.009	200.5± 16.2	108.2± 11.7	28.1± 2.5	71.0± 0.4	42.0± 0.1	94.	13	0.32	26C
				filament F3						
5	0.00001	103.1± 3.6	28.6± 2.5	8.5± 0.9	68.8± 0.2	41.6± 0.0	74.	7072	0.14	3S
5	0.0001	103.1± 3.6	28.6± 2.5	8.5± 0.9	68.8± 0.2	41.6± 0.0	74.	6847	0.16	3S
5	0.001	103.6± 3.6	28.9± 2.5	8.7± 0.9	68.9± 0.3	41.7± 0.0	74.	5055	0.13	3S
5	0.003	105.1± 4.6	29.8± 3.2	9.1± 1.2	69.0± 0.3	41.7± 0.0	74.	1320	0.14	3S
5	0.005	110.1± 7.2	33.1± 4.9	10.5± 1.8	69.4± 0.5	41.7± 0.0	76	42	0.10	32S
10	0.00001	102.8± 4.9	28.4± 3.5	8.2± 1.2	68.8± 0.3	41.6± 0.1	73.	7158	0.18	3S
10	0.0001	102.8± 5.0	28.5± 3.6	8.3± 1.2	68.8± 0.3	41.6± 0.1	73.	7074	0.21	3C
10	0.001	103.2± 4.5	28.6± 3.2	8.4± 1.2	68.8± 0.3	41.6± 0.0	74.	5149	0.19	3S
10	0.003	104.7± 4.8	29.4± 3.3	9.0± 1.3	69.0± 0.3	41.7± 0.0	74.	1209	0.20	3S
10	0.005	110.1± 7.0	32.8± 4.8	10.7± 1.9	69.5± 0.4	41.7± 0.0	76	33	0.09	32S
20	0.00001	108.2± 8.6	32.8± 6.4	9.3± 1.9	69.0± 0.4	41.6± 0.1	75.	4484	0.27	30S
20	0.0001	108.1± 8.3	32.7± 6.2	9.2± 1.8	69.0± 0.4	41.6± 0.1	74.	4460	0.24	
20	0.001	108.7± 7.8	33.0± 5.9	9.5± 1.8	69.0± 0.4	41.6± 0.1	75.	3207	0.28	3S
20	0.003	111.3± 8.7	34.3± 6.4	10.5± 2.1	69.3± 0.4	41.6± 0.1	76.	852	0.26	3S
20	0.005	112.8± 7.2	34.4± 5.0	11.6± 1.9	69.6± 0.4	41.7± 0.1	77.	79	0.20	25C, 30S
20	0.006	119.0± 12.2	38.5± 8.7	13.2± 2.6	70.0± 0.6	41.7± 0.1	79	12	0.14	–
40	0.00001	117.0± 13.3	39.2± 10.2	11.4± 2.8	69.4± 0.6	41.6± 0.1	77.	1724	0.26	30S
40	0.0001	116.0± 12.3	38.4± 9.5	11.1± 2.7	69.4± 0.6	41.6± 0.1	76.	1572	0.22	25C, 30S
40	0.001	120.3± 14.7	41.6± 11.3	12.2± 3.0	69.6± 0.6	41.6± 0.1	77.	1217	0.22	25C
40	0.003	121.8± 12.6	42.2± 9.7	12.9± 2.9	69.8± 0.6	41.6± 0.1	78.	407	0.26	25C
40	0.005	120.4± 9.1	40.2± 6.7	13.2± 2.4	69.9± 0.5	41.7± 0.1	78.	56	0.13	25C
50	0.007	155.2± 7.3	71.0± 6.3	18.3± 0.9	70.7± 0.2	41.6± 0.0	83.	6	0.22	–
70	0.007	117.3± 13.2	35.0± 9.0	11.5± 3.0	68.7± 4.9	41.2± 2.1	81.	20	0.20	25C, 32S
80	0.00001	112.7± 13.6	36.4± 11.4	10.3± 3.4	69.1± 0.6	41.6± 0.1	75.	297	0.35	25C
80	0.0001	119.1± 17.6	42.0± 14.9	11.3± 3.7	69.3± 0.7	41.6± 0.1	76.	405	0.40	25C

Table 1. - continued.

t_{ev}	β	$\lambda_\odot$	α	δ	V_g	V_h	γ	N_s	D_{lim}	i.r.s.
				filament F3 − continuation						
80	0.001	122.4± 17.7	45.1± 15.0	12.2± 3.5	69.3± 0.7	41.6± 0.1	76.	446	0.38	25C
80	0.003	128.2± 15.7	50.4± 13.7	13.7± 3.3	69.5± 0.6	41.6± 0.1	77	277	0.35	–
80	0.0001	119.1± 17.6	42.0± 14.9	11.3± 3.7	69.3± 0.7	41.6± 0.1	76.	405	0.40	25C
80	0.001	122.4± 17.7	45.1± 15.0	12.2± 3.5	69.3± 0.7	41.6± 0.1	76.	446	0.38	25C
80	0.003	128.2± 15.7	50.4± 13.7	13.7± 3.3	69.5± 0.6	41.6± 0.1	77	277	0.35	–
				filament F4						
10	0.00001	213.7± 3.1	109.2± 2.5	21.5± 0.4	69.9± 0.1	42.1± 0.0	106.	5	0.05	–
10	0.0001	197.0± 13.4	97.7± 9.7	20.7± 1.5	70.6± 0.4	41.9± 0.3	100.	6	0.14	–
20	0.00001	202.1± 12.7	101.9± 9.3	20.1± 1.7	70.5± 0.4	41.9± 0.2	101.	152	0.26	–
20	0.0001	202.9± 12.0	102.5± 8.8	20.4± 1.4	70.5± 0.4	41.9± 0.2	101.	165	0.28	–
20	0.001	203.6± 7.5	102.1± 5.9	20.8± 1.1	70.5± 0.3	42.0± 0.1	102.	84	0.13	–
20	0.003	199.2± 11.0	98.8± 8.0	20.6± 1.6	70.6± 0.3	42.0± 0.2	101.	49	0.27	–
40	0.00001	200.8± 14.2	101.9± 10.7	19.7± 1.9	70.7± 0.4	41.9± 0.2	100.	348	0.24	–
40	0.0001	199.6± 14.4	101.2± 10.9	19.6± 1.9	70.7± 0.4	41.9± 0.2	99.	359	0.24	–
40	0.001	201.2± 10.9	102.4± 8.5	19.8± 1.7	70.8± 0.3	41.9± 0.1	100.	195	0.24	–
40	0.003	192.2± 13.9	95.3± 10.1	20.5± 1.5	70.9± 0.3	41.9± 0.2	97.	83	0.33	–
40	0.005	194.5± 7.7	96.9± 6.7	20.7± 0.8	71.0± 0.1	41.9± 0.1	98.	12	0.16	–
50	0.007	194.2± 8.0	96.7± 7.3	20.2± 2.6	71.0± 0.3	42.0± 0.1	98.	20	0.27	–
80	0.00001	200.2± 5.6	94.7± 4.6	19.8± 1.0	69.7± 0.3	42.1± 0.0	106	567	0.20	–
80	0.0001	199.9± 5.4	94.4± 4.5	19.8± 1.0	69.7± 0.3	42.1± 0.0	106.	507	0.18	–
80	0.001	199.2± 6.0	93.9± 4.9	20.1± 0.8	69.8± 0.3	42.1± 0.0	106.	254	0.18	–
80	0.003	193.4± 25.6	104.0± 18.9	16.6± 2.6	70.9± 0.5	41.8± 0.2	90.	179	0.32	–
				filament F5						
70	0.007	186.4± 5.3	83.6± 4.3	20.9± 0.5	70.4± 0.2	42.1± 0.0	102.	336	0.10	–
78	0.007	182.8± 4.7	80.3± 3.6	19.1± 0.5	70.3± 0.2	42.0± 0.0	102.	189	0.10	–
80	0.005	190.5± 6.1	87.2± 5.1	17.8± 1.8	70.0± 0.2	42.1± 0.0	103.	114	0.18	–
80	0.007	188.7± 5.7	86.0± 5.0	17.2± 1.8	70.1± 0.2	42.1± 0.0	103.	123	0.20	–
80	0.009	184.2± 4.4	82.1± 3.9	16.3± 2.6	70.1± 0.3	42.0± 0.0	102.	33	0.21	–

Table 2. Mean orbital characteristics with the dispersion (characterized by the standard deviation) of the predicted annual meteor showers associated with the parent body considered. Notes: t_{ev}, β, and i.r.s - as in Table 1; q - the mean perihelion distance; a - the mean semi-major axis; e - the mean eccentricity; ω - the mean argument of perihelion; Ω - the mean longitude of ascending node; and i - the mean inclination to the ecliptic. Quantities q and a are given in astronomical units and angular elements in degrees.

t_{ev}	β	q	a	e	ω	Ω	i	i.r.s.
				filament F1				
10	0.0001	0.794± 0.041	64.2± 28.3	0.985± 0.008	143.8± 24.4	123.7± 23.8	177.4± 2.0	–
20	0.00001	0.862± 0.057	51.9± 44.5	0.978± 0.009	138.4± 21.8	120.9± 22.7	176.9± 1.9	–
20	0.0001	0.857± 0.075		0.982± 0.010	141.4± 19.1	122.6± 19.0	175.8± 3.1	–
20	0.001	0.856± 0.059	49.8± 44.4	0.982± 0.010	143.7± 18.0	124.9± 19.8	176.2± 2.3	–
20	0.003	0.910± 0.071	46.5± 20.9	0.977± 0.009	135.2± 19.1	117.2± 18.8	177.1± 1.7	–
40	0.00001	0.927± 0.070		0.982± 0.013	155.9± 29.7	139.0± 26.5	175.0± 2.5	–
40	0.0001	0.894± 0.065	65.6± 64.7	0.979± 0.010	141.5± 21.7	127.0± 21.3	176.1± 2.0	–
40	0.001	0.953± 0.067	240.1± 199.5	0.988± 0.012	163.2± 26.8	141.5± 22.2	174.8± 2.2	–
40	0.003	0.978± 0.042	330.6± 234.7	0.996± 0.002	173.6± 5.4	145.7± 5.4	174.2± 0.6	–
40	0.005	0.978± 0.043		0.996± 0.002	170.6± 6.1	142.4± 6.3	174.3± 0.6	–
40	0.007	0.980± 0.045	401.4± 367.1	0.997± 0.002	168.7± 5.6	140.2± 5.8	174.4± 0.5	–
40	0.008	0.981± 0.047		0.997± 0.001	166.0± 4.8	137.0± 4.9	174.4± 0.5	–
50	0.007	0.963± 0.042		0.995± 0.003	151.6± 11.8	122.6± 13.0	174.6± 0.9	20S
60	0.007	0.884± 0.045		0.999± 0.001	104.0± 8.6	69.8± 8.6	175.5± 0.3	–
70	0.007	0.907± 0.041	208.7± 180.1	0.994± 0.004	128.1± 17.5	97.1± 19.7	174.2± 2.0	–
80	0.00001	0.821± 0.064		0.994± 0.005	128.9± 17.2	98.8± 19.0	171.6± 3.3	13C
80	0.0001	0.823± 0.062	206.4± 191.3	0.993± 0.005	129.5± 17.0	99.8± 19.1	171.4± 3.4	13C
80	0.001	0.849± 0.067	209.0± 206.5	0.993± 0.005	134.6± 17.6	106.4± 20.7	170.8± 3.9	13C
80	0.003	0.899± 0.056	146.6± 123.2	0.990± 0.006	141.2± 14.6	119.6± 19.9	168.6± 3.8	15C
80	0.005	0.915± 0.049	118.9±111.9	0.989± 0.006	142.0±15.5	125.1± 21.4	168.3± 3.5	16C
80	0.007	0.927± 0.046	96.9± 56.2	0.987± 0.007	142.9± 18.1	128.9± 24.5	169.0± 3.4	17C, 10S
80	0.009	0.935± 0.038	96.9± 61.5	0.987± 0.006	142.3±16.7	126.0± 21.3	170.6± 3.5	10S
80	0.010	0.953± 0.055		0.989± 0.008	162.3±43.2	137.3± 46.1	174.2± 3.8	–

Table 2. − continued.

t_{ev}	β	q	a	e	ω	Ω	i	i.r.s.
				filament F2				
10	0.00001	0.762± 0.019	132.9± 57.3	0.994± 0.002	264.9± 2.4	243.3± 2.6	174.3± 0.1	–
10	0.0001	0.766± 0.017	130.6± 31.6	0.994± 0.001	264.6± 2.4	243.0± 2.7	174.2± 0.1	–
10	0.001	0.771± 0.016	167.6± 76.0	0.995± 0.002	263.4± 2.1	241.5± 2.5	174.2± 0.1	–
10	0.003	0.776± 0.011		0.996± 0.002	262.1± 1.7	239.8± 2.0	174.1± 0.1	–
10	0.005	0.776± 0.011	342.7±191.9	0.997± 0.001	261.1± 0.9	238.4± 1.0	174.0± 0.0	–
20	0.00001	0.803± 0.035	154.5± 109.3	0.993± 0.004	250.7± 10.5	229.6± 10.5	173.8± 1.0	18C
20	0.0001	0.806± 0.035	146.4± 78.8	0.993± 0.004	250.8± 10.0	229.6± 9.9	173.8± 0.9	18C
20	0.001	0.814± 0.035	163.9± 98.1	0.994± 0.003	250.1± 7.2	228.5± 7.4	173.6± 0.7	18C
20	0.003	0.832± 0.033		0.995± 0.003	246.9± 5.9	224.5± 6.3	173.5± 0.6	14C
20	0.005	0.842± 0.029	280.6± 238.1	0.996± 0.002	244.4± 3.9	221.4± 4.1	173.4± 0.3	14C
20	0.006	0.850± 0.030	384.2± 375.7	0.997± 0.001	242.8± 2.7	219.3± 2.8	173.3± 0.2	14C
40	0.00001	0.848± 0.044	119.3± 75.4	0.991± 0.004	223.9± 15.0	200.5± 16.5	172.4± 2.0	14C
40	0.0001	0.850± 0.044	122.3± 120.8	0.991± 0.004	223.1± 15.2	199.7± 16.7	172.4± 2.1	14C
40	0.001	0.867± 0.044		0.991± 0.004	218.5± 15.8	194.7± 17.4	172.7± 1.9	14C, 24S
40	0.003	0.900± 0.043	146.1±133.8	0.992± 0.004	209.4± 16.5	184.6± 18.1	173.6± 1.6	14C
40	0.005	0.922± 0.038	157.3± 96.5	0.992± 0.004	202.6± 15.4	177.0± 16.6	174.2± 1.3	14C
40	0.007	0.946± 0.033	174.8± 91.4	0.993± 0.003	193.7± 12.4	166.7± 13.1	174.9± 1.0	20S
40	0.008	0.941± 0.034	167.0± 61.8	0.994± 0.002	191.1± 13.4	162.9± 13.6	175.6± 0.8	20S
50	0.007	0.948± 0.039	117.3± 80.7	0.990± 0.005	204.6± 19.4	180.4± 20.5	175.3± 1.7	14C, 20S
70	0.007	0.912± 0.043	103.3± 100.1	0.987± 0.007	206.3± 20.4	182.2± 21.8	175.3± 1.9	14C, 20S
80	0.00001	0.867± 0.066		0.984± 0.008	217.6± 19.2	200.1± 19.3	170.0± 4.2	22S, 18C
80	0.0001	0.863± 0.064	82.9± 75.8	0.985± 0.008	218.2± 16.7	200.5± 17.3	170.1± 4.2	22S, 18C
80	0.001	0.873± 0.067		0.984± 0.008	216.4± 17.9	200.7± 18.7	170.0± 4.1	22S, 18C
80	0.003	0.915± 0.067	60.7± 46.7	0.981± 0.007	206.4± 21.0	199.4± 19.8	168.5± 4.0	23C
80	0.005	0.948± 0.053	53.2± 27.5	0.979± 0.007	198.5± 19.0	199.7± 18.1	168.0± 3.4	24C
80	0.007	0.945± 0.056	53.2± 26.1	0.979± 0.008	202.5± 18.2	203.1± 14.7	169.8± 3.5	24C
80	0.009	0.945± 0.045	53.7± 17.9	0.981± 0.006	196.3± 25.1	199.7± 20.3	169.3± 3.8	26C

Table 2. - continued.

t_{ev}	β	q	a	e	ω	Ω	i	i.r.s.
				filament F3				
5	0.00001	0.800± 0.027	84.9± 31.5	0.989± 0.003	287.2± 8.8	266.0± 8.8	174.1± 0.8	3S
5	0.0001	0.800± 0.027	85.2± 31.0	0.990± 0.003	287.2± 8.9	266.0± 8.8	174.1± 0.8	3S
5	0.001	0.805± 0.027	99.0± 40.8	0.991± 0.003	285.8± 8.0	264.4± 7.9	174.2± 0.7	3S
5	0.003	0.818± 0.033	144.6± 109.5	0.993± 0.002	284.3± 7.2	262.6± 7.1	174.3± 0.7	3S
5	0.005	0.855± 0.048		0.997± 0.002	286.1± 6.3	263.8± 6.3	174.7± 0.5	32S
10	0.00001	0.794± 0.034	86.8± 43.5	0.989± 0.004	293.8± 12.6	272.8± 12.8	173.8± 1.3	3S
10	0.0001	0.794± 0.035	87.6± 42.6	0.989± 0.004	293.6± 12.6	272.7± 12.9	173.8± 1.3	3S
10	0.001	0.800± 0.033	99.4± 51.0	0.990± 0.004	290.8± 11.5	269.5± 11.7	174.0± 1.2	3S
10	0.003	0.817± 0.034	136.9± 66.9	0.993± 0.003	286.8± 8.8	264.8± 8.8	174.4± 0.9	3S
10	0.005	0.858± 0.046		0.996± 0.001	284.8± 5.3	261.9± 5.3	175.3± 0.5	32S
20	0.00001	0.817± 0.049	79.1± 52.4	0.987± 0.006	302.0± 16.4	282.9± 17.3	173.0± 2.3	30S
20	0.0001	0.816± 0.048	80.6± 58.9	0.987± 0.006	301.7± 16.0	282.5± 16.8	173.1± 2.1	30S
20	0.001	0.824± 0.045	84.3± 82.5	0.988± 0.006	300.5± 15.9	281.0± 16.8	173.4± 2.1	3S
20	0.003	0.849± 0.047		0.989± 0.006	298.4± 22.2	278.6± 18.1	174.3± 2.1	3S
20	0.005	0.872± 0.044		0.991± 0.005	301.5± 21.0	278.7± 20.9	176.1± 1.5	25C, 30S
20	0.006	0.904± 0.069		0.988± 0.012	306.4± 20.4	283.3± 21.0	176.7± 1.7	–
40	0.00001	0.859± 0.063	70.8± 61.5	0.984± 0.008	311.1± 22.9	293.7± 23.5	173.4± 2.9	30S
40	0.0001	0.856± 0.061		0.984± 0.007	310.7± 20.5	293.1± 20.8	173.3± 2.9	25C, 30S
40	0.001	0.875± 0.062	69.2± 51.4	0.984± 0.008	309.2± 37.6	294.7± 29.2	173.7± 2.8	25C
40	0.003	0.894± 0.058	79.3± 66.3	0.985± 0.007	310.5± 25.9	292.3± 27.7	174.4± 2.8	25C
40	0.005	0.903± 0.046	94.2± 57.9	0.988± 0.005	305.4± 20.9	284.6± 22.4	175.6± 1.7	25C
50	0.007	0.972± 0.020	40.8± 7.2	0.975± 0.005	335.6± 17.4	333.2± 17.1	173.1± 2.1	–
70	0.007	0.903± 0.056	93.2± 47.6	0.988± 0.006	302.5± 23.2	277.6± 25.2	175.8± 1.8	25C, 32S
80	0.00001	0.832± 0.062		0.986± 0.008	311.2± 17.2	293.9± 19.5	173.2± 3.4	25C
80	0.0001	0.848± 0.070		0.984± 0.009	313.5± 22.8	300.4± 21.0	172.4± 3.6	25C
80	0.001	0.851± 0.070	77.2± 71.5	0.984± 0.009	311.6± 23.7	301.3± 23.0	172.3± 4.0	25C
80	0.003	0.861± 0.059	78.5± 69.1	0.984± 0.008	314.7± 18.9	306.6± 28.7	172.4± 4.1	–

Table 2. - continued.

t_{ev}	β	q	a	e	ω	Ω	i	i.r.s.
				filament F4				
10	0.00001	0.776± 0.020	71.5± 10.0	0.989± 0.002	9.7± 7.8	-12.5± 7.3	178.0± 0.9	–
10	0.0001	0.891± 0.082		0.974± 0.017	20.3± 29.0	2.3± 29.2	175.6± 2.3	–
20	0.00001	0.871± 0.073	59.0± 53.0	0.978± 0.011	29.1± 21.5	12.1± 21.3	175.2± 3.0	–
20	0.0001	0.867± 0.071	66.9± 65.4	0.979± 0.012	28.6± 21.3	11.3± 21.1	175.6± 2.5	–
20	0.001	0.852± 0.045		0.986± 0.007	26.9± 18.2	6.5± 18.4	175.9± 1.9	–
20	0.003	0.874± 0.065	90.9± 56.8	0.985± 0.011	27.5± 17.2	7.2± 16.6	175.6± 2.8	–
40	0.00001	0.894± 0.073		0.978± 0.010	27.3± 19.9	13.6± 20.3	174.7± 3.1	–
40	0.0001	0.903± 0.072	52.1± 40.7	0.977± 0.010	26.5± 19.9	13.4± 20.0	174.5± 3.2	–
40	0.001	0.900± 0.058	56.9± 55.5	0.979± 0.010	26.7± 18.6	13.4± 20.3	174.7± 2.8	–
40	0.003	0.930± 0.066	61.2± 56.3	0.978± 0.010	22.1± 23.4	8.1± 23.0	175.3± 2.6	–
40	0.005	0.928± 0.034	55.2± 18.6	0.982± 0.006	16.1± 14.7	1.1± 13.4	175.4± 1.1	–
50	0.007	0.929± 0.042	74.1± 42.4	0.984± 0.008	24.5± 17.7	10.2± 15.5	174.8± 4.3	–
80	0.00001	0.790± 0.037	358.1±294.7	0.997± 0.002	64.6± 11.9	30.2± 12.0	173.2± 1.8	–
80	0.0001	0.792± 0.035		0.997± 0.002	65.7± 11.0	31.2± 11.5	173.1± 1.7	–
80	0.001	0.796± 0.039		0.997± 0.002	66.9± 11.4	32.4± 12.0	173.7± 1.4	–
80	0.003	0.948± 0.049		0.974± 0.009	359.4± 30.2	11.7± 28.9	171.1± 4.0	–
				filament F5				
70	0.007	0.875± 0.031	451.8± 392.8	0.997± 0.001	70.3± 7.8	34.1± 8.5	175.2± 0.7	–
78	0.007	0.882± 0.032		0.997± 0.002	51.7± 5.5	12.8± 5.8	172.3± 1.0	–
80	0.005	0.859± 0.032		0.996± 0.002	56.3± 7.5	21.0± 9.0	169.3± 3.3	–
80	0.007	0.874± 0.027	294.6± 226.5	0.996± 0.003	53.4± 6.3	18.3± 7.9	168.4± 3.2	–
80	0.009	0.893± 0.022	251.0± 207.8	0.996± 0.003	49.0± 5.4	11.8± 7.2	166.9± 4.6	–

Table 3. Mean geophysical characteristics of the real showers separated from the CAMS video (C) and SonotaCo video (S) databases and identified with at least one of predicted filaments (F1, F2, F3, or F4) of the modeled meteoroid stream of comet C/1964 N1. Notes: Cat.No. - the working number (in this work) of the shower in the C or S catalog (this number serves to relate the real shower to a filament in Tables 1 and 2); $\lambda_{\odot}$ - the mean solar longitude corresponding to the expected maximum of a shower; α and δ - the equatorial coordinates of mean geocentric radiant; V_g and V_h - the mean geocentric and heliocentric velocity; γ - the angular distance of the mean radiant from the Sun at the time corresponding to the $\lambda_{\odot}$ of the maximum; N_s - the number of the real meteors of a given shower selected from the given database; D_{lim} - the threshold value of the Southworth-Hawkins D-discriminant used to separate the meteors of the observed shower; i.p.f. - the predicted filament with which the given real shower is identified. Angular quantities are given in degrees, and velocities in km s^{-1}.

Cat.No.	$\lambda_{\odot}$	α	δ	V_g	V_h	γ	N_s	D_{lim}	i.p.f.
13C	101.5± 7.8	22.1± 6.3	15.6± 2.4	69.1± 1.0	41.8± 0.8	75	13	0.14	F1
14C	195.2± 7.8	96.0± 6.9	27.3± 1.0	70.4± 0.2	41.7± 0.2	100	9	0.10	F2
15C	115.7± 6.8	32.1± 5.0	21.5± 2.7	68.4± 0.7	40.6± 0.5	79	8	0.10	F1
16C	135.6± 12.9	48.3± 10.4	26.1± 3.4	69.5± 0.8	41.0± 0.7	83	20	0.15	F1
17C	143.8± 6.3	57.1± 5.2	28.4± 1.5	69.3± 0.5	40.7± 0.5	83	8	0.10	F1
18C	199.6± 7.3	100.1± 6.2	27.5± 1.0	70.3± 0.4	41.7± 0.3	101	7	0.09	F2
23C	215.7± 6.2	117.6± 5.0	28.4± 1.5	69.8± 0.5	41.4± 0.5	101	9	0.11	F2
24C	210.8± 9.9	116.5± 8.0	28.0± 1.1	70.9± 0.6	41.9± 0.4	97	6	0.10	F2
25C	113.2± 7.4	36.2± 5.5	8.9± 2.1	68.8± 0.5	41.1± 0.5	76	18	0.10	F3
26C	211.5± 8.6	117.3± 6.8	27.0± 1.9	70.9± 0.5	41.8± 0.3	97	9	0.11	F2
3S	101.3± 34.9	35.3± 3.2	8.9± 1.2	69.4± 0.4	41.7± 0.3	65	20	0.08	F3
10S	145.1± 8.8	56.8± 6.8	27.3± 1.7	70.2± 0.4	41.4± 0.5	85	5	0.10	F1
20S	153.8± 81.3	92.2± 5.7	27.2± 0.9	70.5± 0.6	41.7± 0.5	62	10	0.09	F2
22S	221.3± 56.3	102.5± 4.8	28.5± 0.9	70.4± 0.4	42.0± 0.5	120	8	0.07	F2
24S	204.6± 3.6	103.4± 3.3	28.2± 0.6	70.9± 0.4	42.7± 0.3	103	10	0.07	F2
30S	104.0± 32.3	36.0± 3.4	9.0± 1.2	69.3± 0.4	41.6± 0.4	67	24	0.09	F3
32S	105.0± 29.3	35.3± 2.8	8.9± 1.3	69.5± 0.4	41.7± 0.3	69	15	0.06	F3

Table 4. Mean orbital characteristics, with the dispersion, of the real showers separated from the CAMS video (C) and SonotaCo video (S) databases and identified with at least one of predicted filaments (F1, F2, F3, or F4) of the modeled meteoroid stream of comet C/1964 N1. Notes: Cat.No. and i.p.f. - as in Table 3; q - the mean perihelion distance; a - the mean semi-major axis; e - the mean eccentricity; ω - the mean argument of perihelion; Ω - the mean longitude of ascending node; and i - the mean inclination to the ecliptic. Quantities q and a are given in astronomical units and angular elements in degrees.

Cat.No.	q	a	e	ω	Ω	i	i.p.f.
13C	0.838± 0.042	620.8± 498.0	1.001± 0.063	130.7± 6.7	101.5± 7.8	169.0± 3.2	F1
14C	0.905± 0.032	28.6± 16.8	0.960± 0.018	215.7± 6.0	195.2± 7.8	172.6± 1.8	F2
15C	0.898± 0.037	10.9± 5.8	0.900± 0.040	139.3± 7.1	115.7± 6.8	165.5± 2.2	F1
16C	0.961± 0.040	168.2± 358.9	0.928± 0.061	155.5± 11.8	135.5± 12.9	165.8± 2.9	F1
17C	0.964± 0.019	19.1± 27.4	0.899± 0.049	154.6± 5.9	143.7± 6.3	165.6± 2.0	F1
18C	0.891± 0.035	29.1± 19.7	0.957± 0.022	218.2± 6.5	199.6± 7.3	172.0± 1.9	F2
23C	0.869± 0.041	18.9± 13.3	0.931± 0.043	221.8± 6.6	215.7± 6.3	166.7± 2.3	F2
24C	0.937± 0.036	346.1± 505.8	0.970± 0.035	206.9± 10.1	210.7± 9.9	168.1± 1.8	F2
25C	0.854± 0.036	75.8± 231.1	0.944± 0.040	312.5± 5.7	293.2± 7.4	170.7± 1.4	F3
26C	0.940± 0.034	237.2± 431.9	0.963± 0.030	206.1± 9.2	211.4± 8.6	169.5± 2.7	F2
3S	0.857± 0.027	20.6± 35.6	0.992± 0.028	313.4± 4.3	292.2± 4.4	171.1± 1.5	F3
10S	0.983± 0.022	13.2± 15.3	0.954± 0.043	161.8± 9.2	145.1± 8.8	167.4± 1.5	F1
20S	0.907± 0.030	5.9± 14.9	0.967± 0.040	215.6± 6.1	191.8± 6.5	173.2± 1.6	F2
22S	0.883± 0.028	14.3± 26.0	0.981± 0.038	219.6± 4.9	202.2± 5.5	169.9± 1.1	F2
24S	0.857± 0.019	−2.4 ± 24.1	1.041± 0.026	223.4± 3.1	204.6± 3.6	170.5± 1.2	F2
30S	0.860± 0.027	19.8± 32.5	0.983± 0.033	313.7± 4.3	293.0± 4.6	170.9± 1.5	F3
32S	0.860± 0.025	19.7± 33.7	0.995± 0.027	313.9± 3.9	292.3± 4.1	171.1± 1.1	F3

Table 5. The showers from the IAU MDC list of all showers found to be related to the predicted showers with meteoroids originating in comet C/1964 N1. In the first column of the table, the evolutionary time, t_{ev}, and the mark "MDC:" are given. While t_{ev} is applicable to the theoretical shower, mark "MDC:" is applicable to the real shower from the IAU MDC list. In the second column, the P-R-effect parameter β is applicable to the theoretical shower and the IAU MDC number, MDC No., to the real shower. In the third last column of Part 1, the number of theoretical particles used to predict the shower, N_{tp} (applicable to the theoretical shower), and the number of real meteors, N_{real} (applicable to the real shower), identified by the original author to be the members of the shower are given. The value of the Southworth-Hawkins D-discriminant between the mean orbits of both predicted and real showers is given in the last but one column of the first part of the table. The meaning of other symbols is following: $\lambda_{\odot}$ - the mean solar longitude, α and δ - the mean right ascension and mean declination of the geocentric radiant, V_g - the mean geocentric velocity, q - the mean perihelion distance, a - the mean semi-major axis, e - the mean eccentricity, ω - the mean argument of perihelion, Ω - the mean longitude of ascending node, and i - the mean inclination to the ecliptic.

PART 1 - geophysical data								
t_{ev} [kyr]; MDC	β; MDC No.	$\lambda_{\odot}$ [deg]	α [deg]	δ [deg]	V_g [km s^{-1}]	N_{tp}; N_{real}	D_{SH}	source
relation to filament F2								
10	0.00500	214.1	109.5	25.1	69.80	64		this work
MDC:	23	206.0	101.6	26.7	68.80	3	0.194	Jenniskens, 2012
MDC:	23	206.0	104.8	26.9	69.40	7	0.100	Cook, 1973
40	0.00001	201.7	100.0	27.1	70.30	4059		this work
MDC:	23	198.0	93.8	28.1	69.60	31	0.163	Jenniskens et al., 2016a
relation to filament F3								
20	0.00300	111.3	34.3	10.5	69.30	852		this work
MDC:	533	112.6	35.0	9.2	68.85	19	0.078	Kornoš et al., 2014b
40	0.00001	117.0	39.2	11.4	69.40	1724		this work
MDC:	533	119.0	40.1	10.6	69.40	61	0.053	Šegon et al., 2014
40	0.00010	116.0	38.4	11.1	69.40	1572		this work
MDC:	533	119.0	40.1	10.6	69.40	61	0.053	Šegon et al., 2014
40	0.00010	116.0	38.4	11.1	69.40	1572		this work
MDC:	533	119.0	41.5	10.7	68.90	20	0.070	Jenniskens et al., 2016b

Table 5. − continued.

PART 1 - geophysical data; continuation								
t_{ev} [kyr]; MDC	β; MDC No.	$\lambda_{\odot}$ [deg]	α [deg]	δ [deg]	V_g [km s^{-1}]	N_{tp}; N_{real}	D_{SH}	source
relation to filament F5								
80	0.00500	190.5	87.2	17.8	70.00	114		this work
(MDC:	718	206.0	96.9	12.7	68.10	33	0.217	Jenniskens et al., 2016a)
PART 2 - orbital elements								
t_{ev}; MDC	β; No.	q [au]	a [au]	e	ω [deg]	Ω [deg]	i [deg]	source
relation to filament F2								
10	0.00500	0.776	342.7	0.997	261.1	238.4	174.0	this work
MDC:	23	0.731	10.0	0.927	241.7	209.0	172.9	Jenniskens, 2012
MDC:	23	0.770	26.8	0.971	237.0	209.7	173.0	Cook, 1973
40	0.00001	0.848	119.3	0.991	223.9	200.5	172.4	this work
MDC:	23	0.813	11.3	0.957	230.9	198.4	171.2	Jenniskens et al., 2016a
relation to filament F3								
20	0.00300	0.849	102.0	0.989	298.4	278.6	174.3	this work
MDC:	533	0.863		0.939	313.8	292.6	171.8	Kornoš et al., 2014b
40	0.00001	0.859	70.8	0.984	311.1	293.7	173.4	this work
MDC:	533	0.883		0.965	318.0	299.0	171.6	Šegon et al., 2014
40	0.00010	0.856	75.5	0.984	310.7	293.1	173.3	this work
MDC:	533	0.883		0.965	318.0	299.0	171.6	Šegon et al., 2014
40	0.00010	0.856	75.5	0.984	310.7	293.1	173.3	this work
MDC:	533	0.860	10.7	0.952	312.4	292.7	170.4	Jenniskens et al., 2016b
relation to filament F5								
80	0.00500	0.859	337.1	0.996	56.3	21.0	169.3	this work
(MDC:	718	0.726	5.8	0.952	60.8	26.3	159.9	Jenniskens et al., 2016a)